Science Robotics
AAAS

Supplementary Materials for

A bipedal walking robot that can fly, slackline, and skateboard

Kyunam Kim *et al.*

Corresponding author: Soon-Jo Chung, sjchung@caltech.edu

Sci. Robot. **6**, eabf8136 (2021)
DOI: 10.1126/scirobotics.abf8136

The PDF file includes:

Supplementary Text
Sections S1 to S7
Figs. S1 to S3
Tables S1 and S2
References (*74–79*)

Other Supplementary Material for this manuscript includes the following:

Movies S1 to S8

Supplementary Text

Section S1. Experimental data for walking on a loosely-tensioned rope

Figure S1 presents the experimental data for walking on a loosely-tensioned rope. The top plot shows the CoM x position (horizontally away from the rope) and z position (upward), each plotted against the y position (along the rope). The rope is deflected downward under the weight of the robot, which makes the mean z position increase as the robot moves from the center of the rope toward the higher attachment point. A back-and-forth movement is seen in the y direction as the robot takes each step, shifting its CoM from one foot to the other and back, as described in the trajectory of Fig. 5. The middle plot shows the evolution in time of the tracking error in the sagittal and frontal planes. We notice periodic disturbances in the frontal plane caused by the foot advancing to a point on the pulled-down rope, which is at a higher position relative to where the robot stands. The sagittal plane has a small tracking error compared to the frontal plane because there is no disturbance, since the steps are made in the frontal plane. The bottom plot shows the commanded propeller thrust signals with respect to time.

Section S2. Energy consumption and Cost of Transportation analysis

Although energy efficiency is not the focus of the LEO design, the Cost of Transportation (CoT) was analyzed to present the current limitations of such a hybrid locomotion system and to inform future researchers interested in this direction about potential challenges that have to be addressed.

While hovering, LEO consumes an average of 992 W, out of which 933 W are powering the propellers and 59 W are powering the on-board electronics and leg actuators. This power consumption is almost cut in half when LEO is walking on the ground, drawing an average of 544 W, which is split between 445 W for propellers and 99 W for electronics and legs. These power measurements were made by measuring the energy required to recharge LEO's

battery after performing a walking or flying maneuver. Therefore, they include the overall power consumption as well as the battery charge/discharge losses. With the relatively small batteries used on LEO, the resulting flight endurance is about 100 seconds and the walking endurance is about 3.5 minutes. The limiting factor is the 29 Wh capacity of the battery powering the propellers.

In Fig. S2, the CoT for different animals, insects, and robotic systems as well as LEO during its two main locomotion modes are plotted. When walking at a speed of 20 cm/s, the measured CoT for LEO was 108. When flying at 1 m/s, the CoT was 48, and it decreased to 15.5 at the flight speed of 3 m/s. The robots used for comparison have CoT values that are lower than LEO's, but they are lacking LEO's multi-modal capabilities. The data used for the plot is summarized in Table S2 and in (*74*).

Section S3. LEO's nonlinear tracking controller: Exponential convergence proof

The construction of the proof follows (*77*). The closed-loop dynamics is given by:

$$m\ell^2\dot{\omega}_e + k\omega_e + k_I \int_{t_0}^{t} \omega_e \, dt' = \tau_{\text{ext}} \tag{6}$$

where $\omega_e = \dot{\alpha} - \dot{\alpha}_r$ is the composite error term that includes both the angular position and rate errors. By introducing the term $\dot{y} = k_I\omega_e$, we can write Eq. 6 as a linear system with a state-dependent coefficient matrix $\boldsymbol{A}(t)$:

$$\begin{bmatrix} \dot{\omega_e} \\ \dot{y} \end{bmatrix} = \begin{bmatrix} -km^{-1}\ell(t)^{-2} & -m^{-1}\ell(t)^{-2} \\ k_I & 0 \end{bmatrix} \begin{bmatrix} \omega_e \\ y \end{bmatrix} =: \boldsymbol{A}(t) \begin{bmatrix} \omega_e \\ y \end{bmatrix}. \tag{7}$$

where $\ell(t)$ is regarded as an external time-varying term for Eq. 6.

We show that the system in Eq. 7 is contracting (i.e., exponentially converging to a single trajectory globally from any initial condition (*78*)). We construct a positive definite matrix $\boldsymbol{P} = \begin{bmatrix} m & b \\ b & 1 \end{bmatrix}$, with a parameter $b \in (0, \sqrt{m})$. The symmetric matrix $(\boldsymbol{PA})_{\text{sym}} =$

$\frac{1}{2}\left((\boldsymbol{PA})+(\boldsymbol{PA})^\top\right)$ is given by:

$$(\boldsymbol{PA})_{\text{sym}} = \begin{bmatrix} k_I b - k\ell^{-2} & \frac{1}{2}k_I - \frac{1}{2}kbm^{-1}\ell^{-2} - \frac{1}{2}\ell^{-2} \\ \frac{1}{2}k_I - \frac{1}{2}kbm^{-1}\ell^{-2} - \frac{1}{2}\ell^{-2} & -bm^{-1}\ell^{-2} \end{bmatrix}.$$

Note that $(\boldsymbol{PA})_{\text{sym}}$ is negative definite uniformly in time if the following conditions hold:

$$b < kk_I^{-1}\ell^{-2} \quad \text{and} \quad b \in (b_1, b_2), \text{ with } b_1 \text{ and } b_2 \text{ being the roots of } \det\left((\boldsymbol{PA})_{\text{sym}}\right) = 0. \quad (8)$$

Combining these conditions with the condition for positive definiteness of matrix $\boldsymbol{P}$, b needs to be chosen as follows:

$$b \in \left(\max(0, b_1), \min\left(b_2, \frac{k}{k_I\ell^2}, \sqrt{m}\right)\right).$$

We define the generalized virtual displacement vector as $\delta\boldsymbol{z} = [\delta\omega_e, \delta y]^\top$, where $\delta\omega_e$ and δy are infinitesimal displacements at fixed time. We compute the rate of change as follows:

$$\begin{aligned}\frac{d}{dt}\left(\delta\boldsymbol{z}^\top\boldsymbol{P}\delta\boldsymbol{z}\right) &= \delta\boldsymbol{z}^\top\left((\boldsymbol{PA})+(\boldsymbol{PA})^\top\right)\delta\boldsymbol{z} \\ &\leq 2\lambda_{\max}\left((\boldsymbol{PA})_{\text{sym}}\right)\|\delta\boldsymbol{z}\|_2^2 \leq \frac{2\lambda_{\max}((\boldsymbol{PA})_{\text{sym}})}{\lambda_{\max}(\boldsymbol{P})}\left(\delta\boldsymbol{z}^\top\boldsymbol{P}\delta\boldsymbol{z}\right)\end{aligned}$$

where $\lambda_{\max}$ is the maximum eigenvalue of the argument matrix.

From contraction analysis (Lemma 6 in (*77*)), all system trajectories converge exponentially fast to a single trajectory $\delta\boldsymbol{z} \to \boldsymbol{0}$ with a convergence rate of $\frac{2\lambda_{\max}((\boldsymbol{PA})_{\text{sym}})}{\lambda_{\min}(\boldsymbol{P})}$. In the presence of a time-varying disturbance term τ_{ext} with the bounded time derivative $\dot{\tau}_{\text{ext}}$, we obtain the following error bound from Lemma 7 in (*77*):

$$\lim_{t\to\infty}\int_0^{\omega_e}\|\delta\omega_e\|_2 \leq \frac{\sqrt{b^2+1}\,\kappa(\boldsymbol{P})}{-\lambda_{\max}\left((\boldsymbol{PA})_{\text{sym}}\right)}\sup_t\|\dot{\tau}_{\text{ext}}\|_2$$

where $\kappa(\boldsymbol{P})$ is the condition number of $\boldsymbol{P}$. Here, we use the fact that $\|\delta\omega_e\|_2 \leq \|\delta\boldsymbol{z}\|_2$ and that the disturbance appears in the right-hand side of Eq. 7 as $\begin{bmatrix}0 & \dot{\tau}_{\text{ext}}\end{bmatrix}^\top$.

Using hierarchical combination (*78*) between the dynamics of ω_e and $\tilde{\alpha}$, we prove the convergence of $\tilde{\alpha}$ to the following error ball:

$$\lim_{t\to\infty}\int_0^{\tilde{\alpha}}\|\delta\tilde{\alpha}\|_2 \leq \frac{\sqrt{b^2+1}}{k_\alpha}\frac{\kappa(\boldsymbol{P})}{-\lambda_{\max}\left((\boldsymbol{PA})_{\text{sym}}\right)}\sup_t\|\dot{\tau}_{\text{ext}}\|_2$$

By comparing the previous equation with Eq. 4, the η function is defined accordingly. Note here that $\lambda_{\max}\left((\boldsymbol{PA})_{\text{sym}}\right) < 0$ as $(\boldsymbol{PA})_{\text{sym}}$ is negative definite under the conditions mentioned in Eq. 8.

Section S4. Modeling of propeller forces and moments for LEO

Suppose the i-th propeller is exerting a thrust force $\boldsymbol{f}_i$ at its location $\boldsymbol{p}_i$ with respect to the body frame $\mathcal{B}$. The thrust can be modeled as $\boldsymbol{f}_i = f_i\hat{\boldsymbol{z}}_i = c_i\omega_i^2\hat{\boldsymbol{z}}_i$, where c_i is a constant, ω_i is the spin speed, and $\hat{\boldsymbol{z}}_i$ is a unit vector in the direction of the propeller thrust (*79*). At the same time, the propeller is also exerting a moment $\boldsymbol{\tau}_i = (\boldsymbol{p}_i - \boldsymbol{p}_{\text{ref}}) \times \boldsymbol{f}_i \pm \gamma_i \boldsymbol{f}_i = f_i\boldsymbol{\mu}_i$ on the body about a point $\boldsymbol{p}_{\text{ref}}$. For LEO, $\boldsymbol{p}_{\text{ref}}$ is either 1) the ground contact point in case LEO is walking on the ground, or 2) the CoM location if LEO is flying. In both cases, we assume $\boldsymbol{p}_{\text{ref}}$ is on the sagittal plane, that is, its body-y component is zero. The scalar γ_i is a constant capturing the drag moment that becomes scaled by the applied thrust, whose sign is determined by the spin direction of the propeller. If the propellers are vertically oriented, then γ_i is the only source of yaw moment; however, if the propellers are tilted, the moment contribution of γ_i becomes negligible as the tilt angle increases. The vector $\boldsymbol{\mu}_i = (\boldsymbol{p}_i - \boldsymbol{p}_{\text{ref}}) \times \hat{\boldsymbol{z}}_i \pm \gamma_i\hat{\boldsymbol{z}}_i$ points in the direction of the moment, but it is not necessarily a unit vector. We denote the collective moment from all propellers as $\boldsymbol{\tau} = \sum_{i=1}^{4} \boldsymbol{\tau}_i$.

Note that $\boldsymbol{p}_i$ and $\hat{\boldsymbol{z}}_i$ are functions of propeller placement only, and if the propellers remain fixed to the body, these vectors are also constant. Consequently, the propeller thrust force and moment become functions of the propeller speeds only. Therefore, once a solution of Eq. 5 is found, it is transformed into Pulse-Width Modulation (PWM) signals and sent to propeller BLDC motors to physically control their speeds.

Section S5. Derivation of no-slip conditions for moment set definition

Consider again the Inverted Pendulum model (Fig. 3B). We investigate a representative case where no rotation has been applied to the pendulum. Hence, the pendulum is vertical and its angular velocity is zero. In addition, we assume the pendulum has a constant length. Under this scenario, we seek the no-slip conditions derived in terms of ground reaction forces and propeller thrusts.

Following the frame definitions in Fig. 3C, let us define the position coordinates of the propellers with respect to the CoM in the body frame $\mathcal{B}$ as

$$\boldsymbol{p}_1 = [a,\, b,\, c]^\top, \quad \boldsymbol{p}_2 = [a,\, -b,\, c]^\top, \quad \boldsymbol{p}_3 = [-a,\, -b,\, c]^\top, \quad \boldsymbol{p}_4 = [-a,\, b,\, c]^\top,$$

where $a, b, c > 0$. In addition, we let the coordinates of the unit direction vectors of the propeller thrusts as

$$\begin{aligned}
\hat{\boldsymbol{z}}_1 &= \left[-\frac{\sin\delta}{\sqrt{2}},\, -\frac{\sin\delta}{\sqrt{2}},\, \cos\delta\right]^\top, \quad & \hat{\boldsymbol{z}}_2 &= \left[-\frac{\sin\delta}{\sqrt{2}},\, \frac{\sin\delta}{\sqrt{2}},\, \cos\delta\right]^\top, \\
\hat{\boldsymbol{z}}_3 &= \left[\frac{\sin\delta}{\sqrt{2}},\, \frac{\sin\delta}{\sqrt{2}},\, \cos\delta\right]^\top, & \hat{\boldsymbol{z}}_4 &= \left[\frac{\sin\delta}{\sqrt{2}},\, -\frac{\sin\delta}{\sqrt{2}},\, \cos\delta\right]^\top.
\end{aligned}$$

Note that $\boldsymbol{p}_k$ and $\hat{\boldsymbol{z}}_k$ $(k = 1, 2, 3, 4)$ are defined with respect to the body basis whereas the ground reaction force $\boldsymbol{f}_r$ is defined with respect to the inertial basis. However, under the assumption of the pendulum being vertical, these two bases are coincident.

Taking this into account and using Newton's second law on both frontal and sagittal planes, we obtain

$$\begin{aligned}
m\ell\ddot{\alpha}^{(\mathrm{s})} &= f_{rx} + \frac{\sin\delta}{\sqrt{2}}(-f_1 - f_2 + f_3 + f_4) \\
m\ell\ddot{\alpha}^{(\mathrm{f})} &= f_{ry} + \frac{\sin\delta}{\sqrt{2}}(-f_1 + f_2 + f_3 - f_4) \\
0 &= f_{rz} - mg + \cos\delta(f_1 + f_2 + f_3 + f_4)
\end{aligned}$$

With the dynamics of $\alpha^{(\mathrm{s})}$ and $\alpha^{(\mathrm{f})}$ in Eq. 2 and by ignoring the propeller drag moment factor γ_k given a relatively large tilt angle δ, we also obtain

$$m\ell^2\ddot{\alpha}^{(\mathrm{s})} = \left((c+\ell)\frac{\sin\delta}{\sqrt{2}} + a\cos\delta\right)(-f_1 - f_2 + f_3 + f_4)$$
$$m\ell^2\ddot{\alpha}^{(\mathrm{f})} = \left((c+\ell)\frac{\sin\delta}{\sqrt{2}} + b\cos\delta\right)(-f_1 + f_2 + f_3 - f_4)$$

Solving for the friction forces, we have

$$f_{rx} = -\ell^{-1}(f_1 + f_2 - f_3 - f_4)\left(\frac{c\sin\delta}{\sqrt{2}} + a\cos\delta\right)$$
$$f_{ry} = -\ell^{-1}(f_1 - f_2 - f_3 + f_4)\left(\frac{c\sin\delta}{\sqrt{2}} + b\cos\delta\right)$$
$$f_{rz} = mg - (f_1 + f_2 + f_3 + f_4)\cos\delta$$

The no-slip conditions arise from the linear static friction condition as

$$|f_{rx}| \le \eta_s f_{rz}, \quad |f_{ry}| \le \eta_s f_{rz}, \quad f_{rz} \ge 0.$$

By using our previous notation f_z for the net vertical thrust $(f_1 + f_2 + f_3 + f_4)\cos\delta$, the vertical component of the reaction force is re-written in an obvious form as $f_{rz} = mg - f_z$. Note that the condition $f_{rz} \ge 0$ is satisfied during LEO's walking as the net vertical propeller thrust we apply is less than the weight of LEO to prevent the loss of ground contact.

One may obtain the same results from a more general case of a rigid body pendulum whose equations of motion can be derived using the Lagrangian method. Since a rigid body has six degrees-of-freedom, a total of six second-order equations would be obtained. For the no-slip pendulum, three of the equations describe its rotational motion, and the remaining three are solved for the ground reaction forces, all of which have rather complex expressions. With our assumptions, however, the equations are substantially simplified, and the same expressions for $\boldsymbol{f}_r$ can be obtained. Furthermore, a careful examination of these equations reveals that the stance foot does not slip when the net moment about the CoM is zero for the particular case of a point-mass pendulum.

Section S6. Solution of the optimized control allocation

To solve this optimization problem efficiently without a numerical solver, we reparameterize the problem with a single parameter $c = \|\boldsymbol{u}\|_1$. Let $\tilde{\boldsymbol{B}}$ be the $\boldsymbol{B}^{\text{walk}}$ matrix with an additional row of ones, such that $\tilde{\boldsymbol{B}}\boldsymbol{u} = \begin{bmatrix} \boldsymbol{\tau}_d \\ c \end{bmatrix}$ since all elements of $\boldsymbol{u}$ are nonnegative. The new optimization formulation becomes:

$$\begin{aligned} \min \quad & c \\ \text{subject to} \quad & \mathbf{0}_{4\times 1} \leq f_{\text{min}} \mathbb{1}_{4\times 1} \leq \tilde{\boldsymbol{B}}^{-1} \begin{bmatrix} \boldsymbol{\tau}_d \\ 0 \end{bmatrix} + \tilde{\boldsymbol{B}}^{-1} \begin{bmatrix} \mathbf{0}_{3\times 1} \\ c \end{bmatrix} \\ & f_z^d / \cos(\delta) \leq c \end{aligned} \tag{9}$$

where $\mathbf{0}_{n\times 1}$ is a vector of n zeros and $\mathbb{1}_{4\times 1} = \begin{bmatrix} 1 & 1 & 1 & 1 \end{bmatrix}^\top$. Note that the first inequality is taken element-wise. The problem of finding c resumes to the following straightforward inequality:

$$c = \max \left\{ \frac{f_z^d}{\cos(\delta)}, \left(f_{\text{min}} \mathbb{1}_{4\times 1} - \tilde{\boldsymbol{B}}^{-1} \begin{bmatrix} \boldsymbol{\tau}_d \\ 0 \end{bmatrix} \right) \oslash \text{col}_4 \left(\tilde{\boldsymbol{B}}^{-1} \right) \right\}$$

Here, $\text{col}_4(\tilde{\boldsymbol{B}}^{-1})$ refers to the fourth column of $\tilde{\boldsymbol{B}}^{-1}$ and $\oslash$ is the element-wise division. Note that $\text{col}_4(\tilde{\boldsymbol{B}}^{-1})$ is strictly positive from the existence of a $\boldsymbol{u}^+ > \mathbf{0}$ such that $\boldsymbol{B}^{\text{walk}}\boldsymbol{u}^+ = \mathbf{0}$, and thus, the element-wise division operation does not change the direction of the inequality signs in Eq. 9. After obtaining c, $\boldsymbol{u}$ is computed as $\boldsymbol{u} = \tilde{\boldsymbol{B}}^{-1} \begin{bmatrix} \boldsymbol{\tau}_d \\ c \end{bmatrix}$.

Section S7. Propeller tilt angle trade-off

As described in the section "Distributed propellers and motors," the propellers are tilted inwards by the angle $\delta = 25°$ to increase LEO's control authority during ground locomotion at the expense of hover efficiency. Figure S3 shows the effect of varying the tilt angle δ on the hover efficiency as well as the maximum moment while on the ground. Here, the hover thrust efficiency is defined as the net vertical thrust divided by the sum of propeller thrusts in hover. The moments are given for an upright configuration ($\alpha^i = \beta^i = 0$) and include the no-slip constraint

(with a friction coefficient of 0.84) as developed for $\mathcal{T}^{\mathrm{walk,no-slip}}$. As seen in Fig. S3, the control effectiveness at $\delta = 25^{\circ}$ is enhanced substantially, while keeping the hover thrust losses low. This angle could be adjusted or actively controlled to optimize LEO for a specific use case.

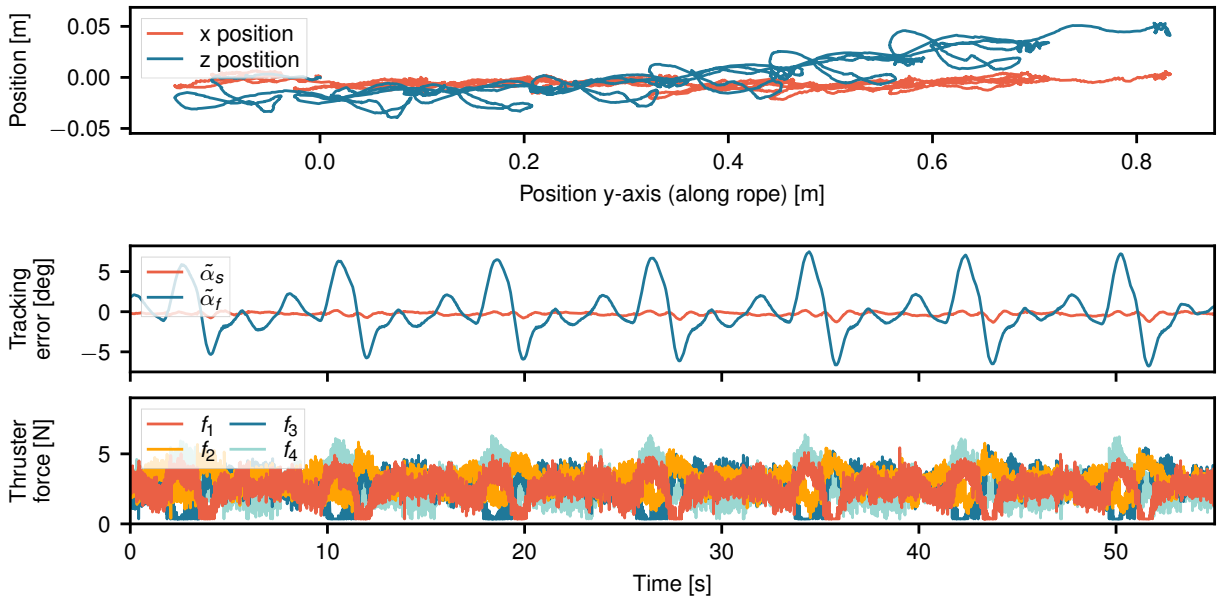

Fig. S1. Experimental data for walking on a loosely-tensioned rope.

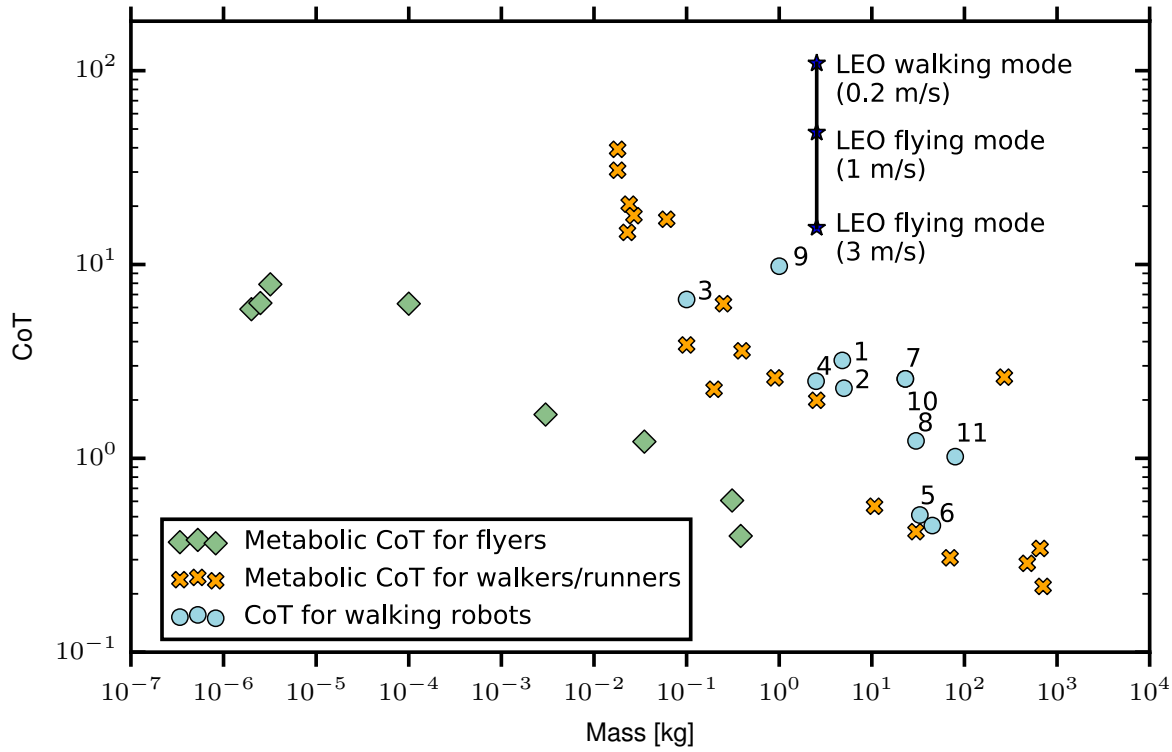

Fig. S2. Mass vs. Cost of Transportation for different walkers, flyers, and robots. The data are provided in Table S2 and in (*74*). The solid line between the data points of LEO represents a range of CoT achievable by combining the two locomotion modes of LEO.

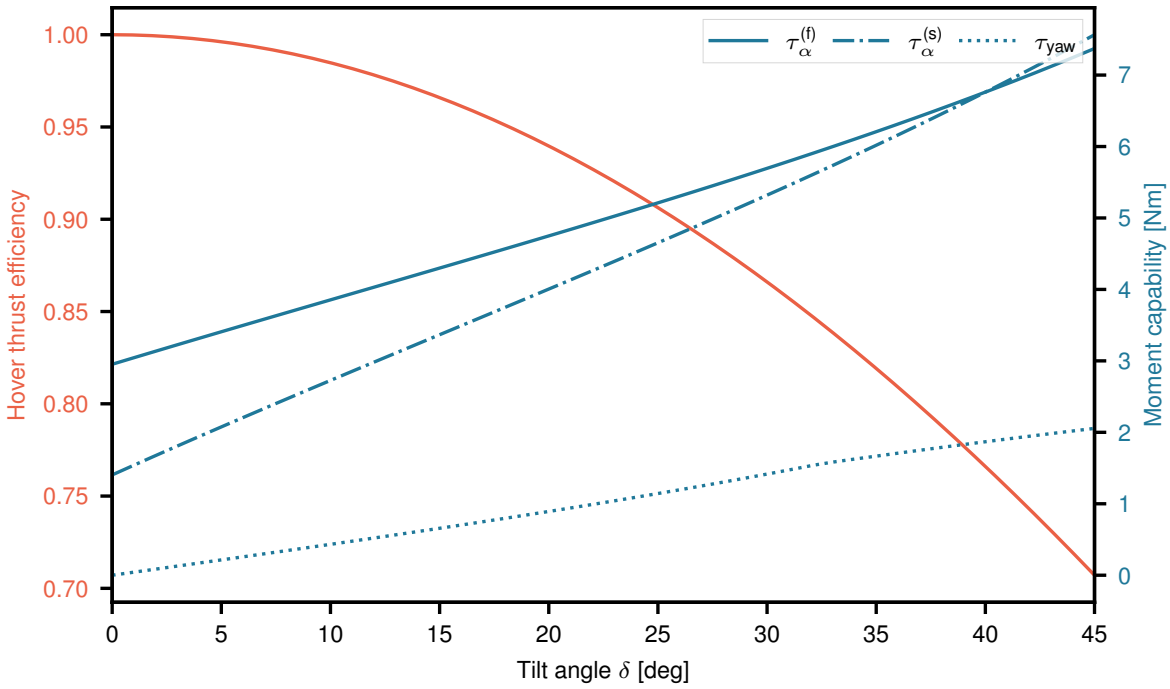

Fig. S3. Propeller tilt angle influence on hover efficiency and control authority.

Component	Reference	Specifications
Leg motors (swing & extension)	MKS HBL599	73.1 g, 4.1 Nm, 2.1 RPS (0.08 s/60°)
Leg motors (ad/abduction)	Hitec HSB-9381TH	78 g, 3.3 Nm, 1.2 RPS (0.14 s/60°)
Propeller motors	Garila X2508	2200kv
Propellers	HQ prop 6x4.5x3	
Propeller motor controller	Holybro Tekko32	35A 4-in-1 3-6S ESC
Microcontroller	STM32F722RE	216 MHz ARM Cortex-M7, 256kB SRAM, 512KB Flash
IMU	ICM-20602	range: $\pm$2000°/s, $\pm$16 g, noise: $0.004°/s/\sqrt{\text{Hz}}$, 100 $\mu g/\sqrt{\text{Hz}}$
VIO camera	Intel Realsense T265	55 g, 163° FoV, on-board VIO processing
Embedded computer	NanoPC-T4	2x2GHz + 4x1.5GHz, 4GB RAM, PCIe SSD, USB 3.0, 802.11ac WiFi, 63 g
Battery for propellers	Tattu R-line 6S	1300 mAh (29 Wh), 155 g, 95C discharge
Battery for legs & electronics	HRB 2S	2700 mAh (20 Wh), 110 g, 10C discharge
Remote control receiver	Graupner GR-12L	2.4 GHz digital RC receiver

Table S1: **LEO's components specifications.**

Robots	Mass [kg]	Speed [m/s]	CoT
1. Stanford Dogoo	4.8	0.9	3.20
2. Minitaur	5	1.5	2.30
3. Salto-1P	0.1	3.6	6.60
4. Jerboa	2.5	1.52	2.50
5. MIT Cheetah 2	33	6.0	0.51
6. MIT Cheetah 3	45	N/A	0.45
7. StarIETH	23	0.7	2.57
8. ANYMAL	30	0.8	1.23
9. Cheetah Cub	1	1.4	9.80
10. XRL	23	1.54	2.57
11. DURUS	79.5	0.6	1.02

Table S2: **Mass, speed, and Cost of Transportation for different walking/jumping robots.** (adapted from (*75, 76*).)